MADRID
inter.noise 2019
June 16 - 19
NOISE CONTROL FOR A BETTER ENVIRONMENT

Impact of the Green function in acoustic analogies for flow noise predictions at low Mach number

Trafny, Nicolas[1]
Serre, Gilles[2]
Naval Group, Naval Research
199 Avenue Pierre-Gilles de Gennes, 83190 Ollioules, France

Cotte, Benjamin[3]
IMSIA, ENSTA ParisTech, CNRS, CEA, EDF, Institut Polytechnique de Paris
828 Boulevard des Maréchaux, 91120 Palaiseau, France

Mercier, Jean-François[4]
POEMS, ENSTA ParisTech, CNRS, INRIA, Institut Polytechnique de Paris
828 Boulevard des Maréchaux, 91120 Palaiseau, France

ABSTRACT

It is known that hydrodynamic noise can be a major contribution to the total sound radiated by a ship. It is in part attributed to the interaction between turbulent eddies with appendages and marine propeller blades. Because hydrodynamics is associated with very low Mach numbers, direct noise computation methods are too expensive. Other approaches must be chosen, based on acoustic analogies which consist first in modeling the incompressible turbulent flow and then in computing the noise radiated by this flow. We focus on Lighthill's wave equation, solved using the free space Green function or a tailored Green's function in presence of an arbitrary geometry. Unlike many studies from the literature where the impact of the chosen turbulent model is evaluated over a semi-infinite plate, the objective of this study is to evaluate the impact of the chosen Green function on the predicted broadband flow noise for a fixed semi-empirical turbulence model. The impact of the chosen tailored Green function on the radiated noise spectra and directivity diagrams is evaluated considering various analytical and numerical tailored Green's functions.

Keywords: Hydrodynamic noise, tailored Green's function, Lighthill equation
I-INCE Classification of Subject Number: 12

[1] nicolas.trafny@ensta-paristech.fr
[2] gilles.serre@naval-group.com
[3] benjamin.cotte@ensta-paristech.fr
[4] jean-francois.mercier@ensta-paristech.fr

1. INTRODUCTION

Hydrodynamic noise is generally generated by a concentrated region of turbulence surrounding a solid boundary or by a flow instability. The rewriting of the Navier-Stokes and continuity equations into an inhomogeneous wave equation is the starting point of acoustic analogies. The common method of resolution of these analogies is based on the formalism of the Green functions. Thus, the computation is, in general, done in two independent steps. The first one is the modeling of the turbulent flow in the entire region of turbulence and the second one is the computation of the Green function.

Numerical simulations of the turbulent flow are too expensive for the usual characteristics of hydrodynamic noise - low Mach number and high Reynolds number - and there are very little experimental data available. However, under these latter conditions, the total noise radiated by a foil would be dominated by the edge noise produced by the turbulence fluctuations which pass over the edges and are scattered in the far field. These can be the turbulent boundary layer fluctuations for trailing edge noise, or the inflow turbulence for leading edge noise. In this context, the diffraction theory, which consider the flow passing over a semi-infinite plate, is widely used to compute edge noise [1–3]. The impact of the real geometry is then lost because this theory does not easily extend to an arbitrary Green's function. On the contrary, volumic formulations, based for example on the work of Doak [4], allow us to use an exact Green's function by canceling surface integrals. Unlike many studies which investigate the impact of the turbulence model [5, 6], the objective of this work is to present a semi-analytical model allowing the investigation of the impact of the Green function, which can be determined analytically or numerically. This model will be applied to trailing edge noise prediction in air and compared to either the diffraction theory or experimental data.

First, we will derive the broadband flow induced noise prediction model in Section 2. Then we will introduce the tailored Green function in Section 3 and the semi-analytical turbulence model in Section 4. Finally, radiated noise spectra and directivity diagrams obtained with the diffraction theory and the volumic formulation are shown in Section 5.

2. BROADBAND FLOW INDUCED NOISE PREDICTION MODEL

2.1. Derivation of the general equation

In the context of hydrodynamic noise studies, the flow is supposed to be incompressible, at high Reynolds and low Mach numbers. Neglecting cavitation and vibration, the Lighthill equation can be written for the pressure in the frequency domain under the following form:

$$(\nabla^2 + k_0^2)\widehat{p}(\mathbf{x}, \omega) = -\frac{\partial^2 \widehat{T_{ij}}}{\partial x_i \partial x_j}, \tag{1}$$

where $k_0 = \omega/c_0$ is the acoustic wave-number, with ω the angular frequency and c_0 the speed of sound, $\widehat{T_{ij}} = \rho_0 \widehat{u_i u_j}$ is the incompressible Lighthill tensor, ρ_0 is the fluid density, u_i is the flow velocity and the superscript $\widehat{\ }$ denotes the frequency Fourier transform which is defined for a function f by:

$$\widehat{f}(\omega) = \frac{1}{2\pi} \int_{-\infty}^{\infty} f(t) e^{-i\omega t} dt. \tag{2}$$

Using the Green function formalism in presence of hard wall surfaces, the integral formulation of the inhomogeneous wave equation, or Green's formula, can be derived [7]:

$$\begin{aligned}\hat{p}(\mathbf{x},\omega) = &-\int_V \frac{\partial^2 \widehat{T_{ij}}}{\partial y_i \partial y_j}\widehat{G}(\mathbf{x},\mathbf{y},\omega)d^3\mathbf{y} \\ &+\oint_\Sigma \left(\widehat{p}(\mathbf{y},\omega)\nabla\widehat{G}(\mathbf{x},\mathbf{y},\omega) - \widehat{G}(\mathbf{x},\mathbf{y},\omega)\nabla\widehat{p}(\mathbf{y},\omega)\right)\cdot\mathbf{n}dS(\mathbf{y}),\end{aligned} \tag{3}$$

where Σ and V are respectively the obstacle and the turbulence volume, $\mathbf{n}$ is taken in the outward direction from the solid and the Green function $\widehat{G}$ is the causal solution at $\mathbf{x} = (x_1, x_2, x_3)$ of the wave equation generated by an impulsive point source at $\mathbf{y} = (y_1, y_2, y_3)$, that is defined by:

$$(\nabla^2 + k_0^2)\widehat{G}(\mathbf{x},\omega) = \delta(\mathbf{x}-\mathbf{y}). \tag{4}$$

The Green function can be chosen in order to take into account the boundaries' geometry. A solution $\widehat{G_T} = \widehat{G_0} + \widehat{G_s}$, with $\widehat{G_0}$ the Green function in free space and $\widehat{G_s}$ the scattered one, of Equation 4 that satisfies the rigid wall boundary condition

$$\nabla\widehat{G_T}(\mathbf{x},\mathbf{y},\omega)\cdot\mathbf{n} = 0, \quad \forall\mathbf{y}\in\Sigma, \tag{5}$$

is called a tailored Green's function to Σ and can be computed independently of the flow. If a tailored Green's function is chosen in Equation 3 and if the wall boundaries are supposed rigid such that:

$$\nabla\widehat{p}(\mathbf{y},\omega)\cdot\mathbf{n} = 0, \quad \forall\mathbf{y}\in\Sigma, \tag{6}$$

the surface integral vanishes and the Doak formula [4] is obtained:

$$\widehat{p}(\mathbf{x},\omega) = -\int_V \frac{\partial^2 \widehat{T_{ij}}}{\partial y_i \partial y_j}\widehat{G_T}(\mathbf{x},\mathbf{y},\omega)d^3\mathbf{y}. \tag{7}$$

At this point, no hypothesis has been made on the geometry of the solid boundaries. In order to compute the far-field noise it is then necessary to evaluate both the tailored Green function and the source term separately.

2.2. The diffraction theory for edge noise prediction

Another class of prediction models for broadband edge noise, such as the one derived by Chase [8] and Chandiramani [1], consider a semi-infinite rigid plate. In this formulation, the calculation of the edge noise is formulated as a diffraction problem of the free field hydrodynamic pressure $\widehat{p_I}$ that would be produced by the same turbulent flow if the surface were absent [3]. The governing equation of the diffraction theory is then [3] :

$$\begin{aligned}\widehat{p}(\mathbf{x},\omega) &= -\oint_\Sigma \widehat{G_T}(\mathbf{x},\mathbf{y},\omega)\nabla\widehat{p_I}(\mathbf{y},\omega)\cdot\mathbf{n}dS(\mathbf{y}) \\ &= -\int_{-\infty}^{0}\int_{-\infty}^{\infty}\left[\widehat{G_s}(\mathbf{x},\mathbf{y},\omega)\right]\frac{\partial\widehat{p_I}}{\partial y_2}(\mathbf{y},\omega)dy_1dy_3,\end{aligned} \tag{8}$$

where $\left[\widehat{G_s}(\mathbf{x},\mathbf{y},\omega)\right]$ is the jump in the value of $\widehat{G_s}$ across the half-plane and the coordinate system is defined in Figure 1. Note that $\left[\widehat{G_0}\right]$ vanishes so the only contribution is from

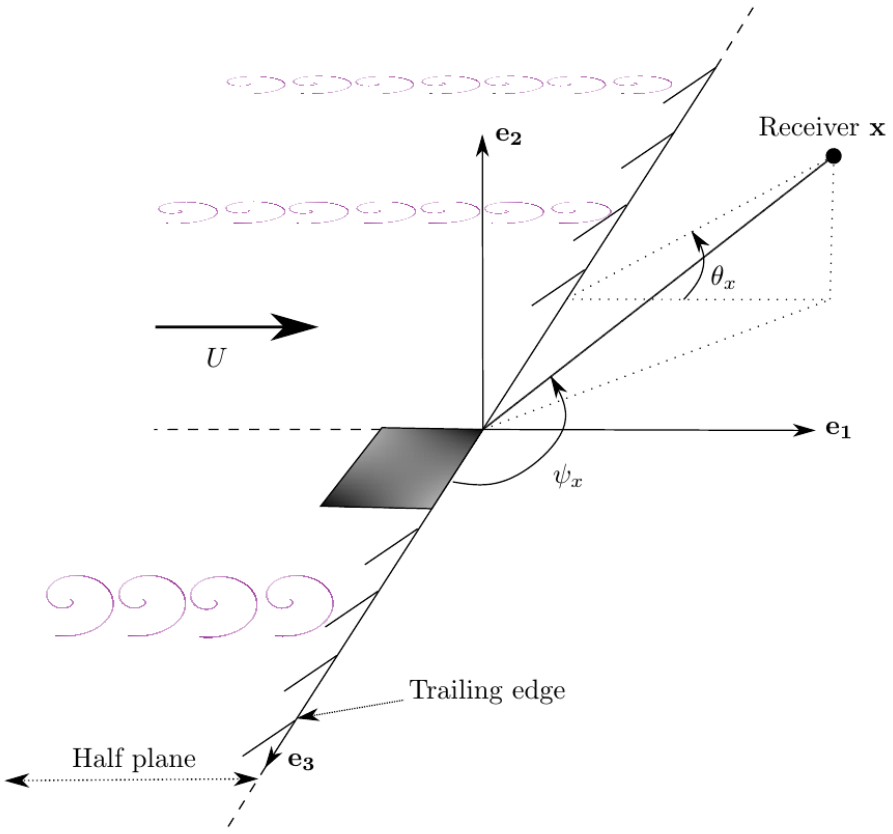

Figure 1: Coordinates for trailing edge noise prediction.

the scattered part of the Green function. Contrary to Equation 3, the pressure gradient in the surface integral is not zero because $\widehat{p_I}$ is not the wall pressure. The presence of the turbulence volume is only accounted for in the computation of the pressure $\widehat{p_I}$ which means that the direct component of the radiated noise is neglected [3]. This formulation is widely used because it combines low computation cost and good agreement with experimental data. It is therefore considered as a benchmark in this study. To that end, we have to start by deriving the equations for the noise spectrum in both approaches under the very same assumptions. Also, we will apply it to the trailing edge noise prediction only. The derivations relative to the diffraction theory will be denoted as *surfacic* approaches whereas the derivations relative to the Doak equation will be denoted as *volumic* approaches.

2.3. Power spectral density of acoustic pressure for mean-shear turbulence

In order to establish a far field noise prediction model for an arbitrary geometry, we look for a comparison between the volumic formulation (Equation 7), and the surfacic formulation (Equation 8). It is then necessary to use the same turbulence model in both formulations. In trailing edge noise study, it is usual [9, 10] to decompose the velocity field into a mean component U_i and a fluctuation u_i' such that $u_i = U_i + u_i'$. Also, it is common to consider that only the transverse mean shears $\partial U_1/\partial y_2$ is non zero and to neglect second order fluctuation terms. These assumptions yield [10]

$$\frac{\partial^2 \widehat{T_{ij}}}{\partial y_i \partial y_j} = 2\rho_0 \frac{\partial U_1}{\partial y_2} \frac{\partial \widehat{u_2'}}{\partial y_1}, \tag{9}$$

so that Equation 7 can be written :

$$\widehat{p}(\mathbf{x},\omega) = -\int_V 2\rho_0 \frac{\partial U_1}{\partial y_2}\frac{\partial \widehat{u_2'}}{\partial y_1}\widehat{G}_T(\mathbf{x},\mathbf{y},\omega)d^3\mathbf{y}. \tag{10}$$

In this study V corresponds to the turbulent boundary layers on the pressure and suction sides. By integrating by part, we can transfer the y_1 derivative to the Green function:

$$\widehat{p}(\mathbf{x},\omega) = -\int_V 2\rho_0 \widehat{u_2'}(\mathbf{y},\omega)\frac{\partial U_1}{\partial y_2}\frac{\partial \widehat{G}_T}{\partial y_1}d^3\mathbf{y}. \tag{11}$$

Considering chordwise and spanwise mean shear as negligible, Equation 11 remains valid for an arbitrary geometry. The power spectral density of the volumic formulation given by Equation 11 reads:

$$\begin{aligned} S_{pp}^{(V)}(\mathbf{x},\omega) &= \langle \widehat{p}(\mathbf{x},\omega)\widehat{p}^*(\mathbf{x},\omega)\rangle \\ &= \int_{V(\mathbf{y})}\int_{V(\mathbf{z})} 4\rho_0^2 \widehat{\phi}_{22}(\mathbf{y},\mathbf{z},\omega)\frac{\partial U_1}{\partial y_2}\frac{\partial U_1}{\partial z_2}\frac{\partial \widehat{G}_T}{\partial y_1}(\mathbf{x},\mathbf{y},\omega)\frac{\partial \widehat{G}_T^*}{\partial z_1}(\mathbf{x},\mathbf{z},\omega)d^3\mathbf{y}d^3\mathbf{z}, \end{aligned} \tag{12}$$

where $\widehat{\phi}_{22}(\mathbf{y},\mathbf{z},\omega) = \langle \widehat{u_2'}(\mathbf{y},\omega)\widehat{u_2'^*}(\mathbf{z},\omega)\rangle$ is the upwash velocity spectrum and where the superscript V stands for volumic. On the other hand, the power spectral density of the surfacic formulation spectrum has been derived by Chase [2] for a half-infinite plane,

$$S_{pp}^{(S)}(\mathbf{x},\omega) = \frac{L\sin^2(\theta_x/2)\sin(\psi_x)}{2\pi c_0|\mathbf{x}|^2}\int_{-\infty}^{\infty}\frac{\widetilde{\phi}_{pp}(k_1,k_3=0,\omega)}{|k_1|}dk_1, \tag{13}$$

where L is the airfoil span, θ_x and ψ_x are defined in Figure 1, and $\widetilde{\phi_{pp}}$ is the wall pressure spectrum. The wall pressure spectrum can be determined for instance from the semi-analytical Blake-TNO model [9, 10] which expresses $\widetilde{\phi_{pp}}$ as a function of $\widetilde{\phi_{22}}$. The space Fourier transform of a function $\widehat{g}(r_1,r_3,\omega)$ is defined by :

$$\widetilde{g}(k_1,k_3,\omega) = \frac{1}{4\pi^2}\int_{-\infty}^{\infty}\widehat{g}(r_1,r_3,\omega)e^{-i(k_1r_1+k_3r_3)}dr_1dr_3. \tag{14}$$

In order to compare both approaches, we need to derive a turbulence model that can be expressed in either the Fourier and the physical space since $S_{pp}^{(V)}$ depends on $\widehat{\phi}_{22}$ while $S_{pp}^{(S)}$ depends on $\widetilde{\phi}_{pp}$. Note that in the diffraction theory it is the jump of the value of $\widehat{G}_S$ that matters, whereas in the volumic approach it is the derivative of $\widehat{G}_T$ with respect to y_1, as investigated in Section 5.

3. ANALYTICAL TAILORED GREEN'S FUNCTIONS

The determination of a tailored Green's function to a given geometry is of great importance in the volumic formulation. It can be obtained, a priori and independently of the turbulent flow simulation, numerically for complex geometries or analytically for simple ones and in the compact approximation [3]. In the acoustic far field and considering a source near the edge, the Green's function tailored to the half-plane $(x_1 < 0, x_2 = 0)$ is [11] :

$$\widehat{G}_{HP}(\mathbf{x},\mathbf{y},\omega) = \frac{-e^{ik_0|\mathbf{x}-y_3\mathbf{i_3}|}}{4\pi|\mathbf{x}-y_3\mathbf{i_3}|} - \frac{\sqrt{k_0 r_x}\sin(\theta_x/2)\sqrt{r_y}\sin(\theta_y/2)}{\pi\sqrt{2\pi i}|\mathbf{x}-y_3\mathbf{i_3}|^{3/2}}e^{ik_0|\mathbf{x}-y_3\mathbf{i_3}|}, \quad k_0|\mathbf{y}| \ll 1, \tag{15}$$

where $\mathbf{x} = (R_x, \theta_x, \psi_x) = (r_x, \theta_x, x_3)$ and $\mathbf{y} = (R_y, \theta_y, \psi_y) = (r_y, \theta_y, y_3)$ are respectively the receiver and the source position expressed in the spherical and cylindrical coordinates described in Figure 1. The term $\sqrt{r_y}\sin(\theta_y/2)$ is often denoted $\varphi^*(\mathbf{y})$ and can be assimilated to the velocity potential of incompressible flow around the edge [3]. Howe [12] extended this Green function to a finite chord profile by considering the multiple scattering between waves diffracted by both the leading and trailing edges :

$$\begin{aligned}
\widehat{G}_{MS}(\mathbf{x},\mathbf{y},\omega) &= \widehat{G}_{HP}(\mathbf{x},\mathbf{y},\omega) + \widehat{G}_{LE}(\mathbf{x},\mathbf{y},\omega) + \widehat{G}_{TE}(\mathbf{x},\mathbf{y},\omega),\\
\widehat{G}_{LE} &= \frac{\sqrt{k_0 \sin\psi_x}\varphi^*(\mathbf{y}) e^{ik_0(|\mathbf{x}'|+c\sin\psi_x)}}{i\pi^{3/2}|\mathbf{x}|(1+e^{2ik_0c\sin\psi_x}/2\pi i k_0 c\sin\psi_x)} \mathcal{F}\left(\sqrt{\frac{k_0 c\sin\psi_x\cos^2(\theta_x/2)}{\pi}}\right),\\
\widehat{G}_{TE} &= \frac{-\varphi^*(\mathbf{y}) e^{ik_0(|\mathbf{x}|+2c\sin\psi_x)}}{\pi^2\sqrt{2ic}|\mathbf{x}|(1+e^{2ik_0c\sin\psi_x}/2\pi i k_0 c\sin\psi_x)} \mathcal{F}\left(2\sqrt{\frac{k_0 c\sin\psi_x\sin^2(\theta_x/2)}{\pi}}\right),
\end{aligned} \tag{16}$$

where $\widehat{G}_{HP}$ is the Green's function given by Equation 15, c is the chord of the plate and $\mathcal{F}(x) = g(x) + if(x)$ is the Fresnel auxiliary function with

$$\begin{aligned}
f(x) &= \frac{1+0.926x}{2+1.792x+3.104x^2},\\
g(x) &= \frac{1}{2+4.142x+3.492x^2+6.670x^3}.
\end{aligned} \tag{17}$$

These two Green's functions are essential in the diffraction theory. Because they both depend on the source position $\mathbf{y}$ in the same way, Howe [12] expressed the power spectral density based on the multiple scattering Green's function as:

$$S^{(S)}_{pp,MS}(\mathbf{x},\omega) = \left|\frac{\widehat{G}_{MS}(\mathbf{x},\mathbf{y},\omega)}{\widehat{G}_{HP}(\mathbf{x},\mathbf{y},\omega)}\right|^2 S^{(S)}_{pp,HP}(\mathbf{x},\omega), \tag{18}$$

with $S^{(S)}_{pp,HP}$ the power spectral density based on the half plane Green's function. Furthermore, by applying the half plane Green function in the volumic formulation, we obtain the model originally developed by Ffowcs Williams and Hall [13] for trailing edge noise prediction.

4. SEMI-ANALYTICAL TURBULENCE MODEL

In order to compare both approaches, we have to ensure that the same expression for the upwash velocity spectrum is used. Thus, a simplified model is built for homogeneous and isotropic boundary layer scaled by a XFoil simulation over a NACA 0012 profile. The starting point is the Blake-TNO model [10], considering an homogeneous turbulence only in the directions $\mathbf{e_1}$ and $\mathbf{e_3}$:

$$\widetilde{\phi_{22}}(k_1, y_2, z_2, k_3, \omega) = \overline{u_2'^2} L_2(y_2)\delta(y_2 - z_2)\widetilde{\phi}^{(1,3)}_{22}(k_1, k_3)\phi_m(\omega - U_c k_1) \tag{19}$$

where $\widetilde{\phi}^{(1,3)}_{22}(k_1, k_3)$ is the anisotropic von Kármán spectrum [10], $\overline{u_2'^2}$ is the variance of the turbulence fluctuations and ϕ_m is the moving axis spectrum [14]. In order to express

the upwash velocity spectrum in the physical space, we look for a separable form for $\widetilde{\phi}_{22}^{(1,3)}(k_1, k_3)$ which is possible for an isotropic turbulence. Integrating over k_3 yields [15]:

$$\widetilde{\phi}_{22}^{(1)}(k_1) = \int_{-\infty}^{\infty} \widehat{\phi}_{22}^{(1,3)}(k_1, k_3) dk_3 = \frac{4}{15 k_e \sqrt{\pi}} \frac{\Gamma(11/6)}{\Gamma(7/3)} \frac{1 + 8/3\,(k_1/k_e)^2}{\left(1 + (k_1/k_e)^2\right)^{(11/6)}}, \tag{20}$$

where k_e is the energy bearing wavenumber. Then, under the frozen turbulence assumption and assuming an exponential decay with respect to the separation [14], the von Kármán spectrum can be expressed in the physical space by

$$\begin{aligned} \widehat{\phi}_{22}^{(1)}(r_1, \omega) &= \int_{-\infty}^{\infty} \widetilde{\phi}_{22}^{(1)}(k_1) \phi_m(\omega - U_c k_1) e^{-ik_1 r_1} dk_1 \\ &= \int_{-\infty}^{\infty} \widetilde{\phi}_{22}^{(1)}(k_1) e^{-\gamma k_1 r_1} \delta(\omega - U_c k_1) e^{-ik_1 r_1} dk_1 \\ &= \frac{\widetilde{\phi}_{22}^{(1)}(\omega/U_c)}{U_c} e^{-i\omega r_1/U_c} e^{-\gamma \omega r_1/U_c}, \end{aligned} \tag{21}$$

where γ is an empirical parameter of order 0.2 to 0.3 and $r_i = y_i - z_i$. When $\gamma\omega/U_c$ is sufficiently high, $\widehat{\phi}_{22}^{(1)}(r_1, \omega) \approx L_1(\omega)\delta(r_1)$ with L_1 the longitudinal integral length scale defined by :

$$L_1(\omega) = \int_0^{\infty} \widehat{\phi}_{22}^{(1)}(r_1, \omega) dr_1 = \frac{\widetilde{\phi}_{22}^{(1)}(\omega/U_c)}{\omega} \frac{1}{(\gamma + i)}. \tag{22}$$

In the transverse direction, we assume an homogeneous turbulence and a Gaussian correlation function such as defined by Blake [16] :

$$\widehat{\phi}_{22}^{(3)}(r_3, \omega) = e^{-(y_3 - z_3)^2/\lambda_3^2} \approx L_3(\omega)\delta(r_3), \tag{23}$$

with,

$$L_3(\omega) = \int_0^{\infty} \widehat{\phi}_{22}^{(3)}(r_3, \omega) dr_3 = \frac{\sqrt{\pi}}{2} |\lambda_3|, \tag{24}$$

where λ_3 is a transverse correlation length scale given by Corcos [17] for a boundary-layer over a rough surface :

$$\lambda_3 = 1.4 \frac{U_c}{\omega}. \tag{25}$$

The Fourier transform of $R_{22}^{(3)}$ yields to the transverse velocity spectrum :

$$\widetilde{\phi}_{22}^{(3)}(k_3) = \frac{\lambda_3}{2\sqrt{\pi}} e^{-(\lambda_3 k_3)^2/4}. \tag{26}$$

Finally, for an homogeneous and isotropic turbulence

$$\widehat{\phi_{22}}(r_1, y_2, z_2, r_3, \omega) = \overline{u_2'^2} L_2(y_2)\delta(r_2) L_1(\omega)\delta(r_1) L_3(\omega)\delta(r_3), \tag{27}$$

and

$$\widetilde{\phi_{22}}(k_1 = \omega/U_c, y_2, z_2, k_3, \omega) = \overline{u_2'^2} L_2(y_2)\delta(r_2) \frac{\widetilde{\phi}_{22}^{(1)}(\omega/U_c)}{U_c} \widetilde{\phi}_{22}^{(3)}(k_3). \tag{28}$$

The main advantage of this simplified model is that it can be expressed in the space domain to be used in Equation 12 and in the Fourier domain to be used in Equation 13. Note that the dependence of $\widetilde{\phi_{22}}$ on k_3 is different in Equations 19 and 28.

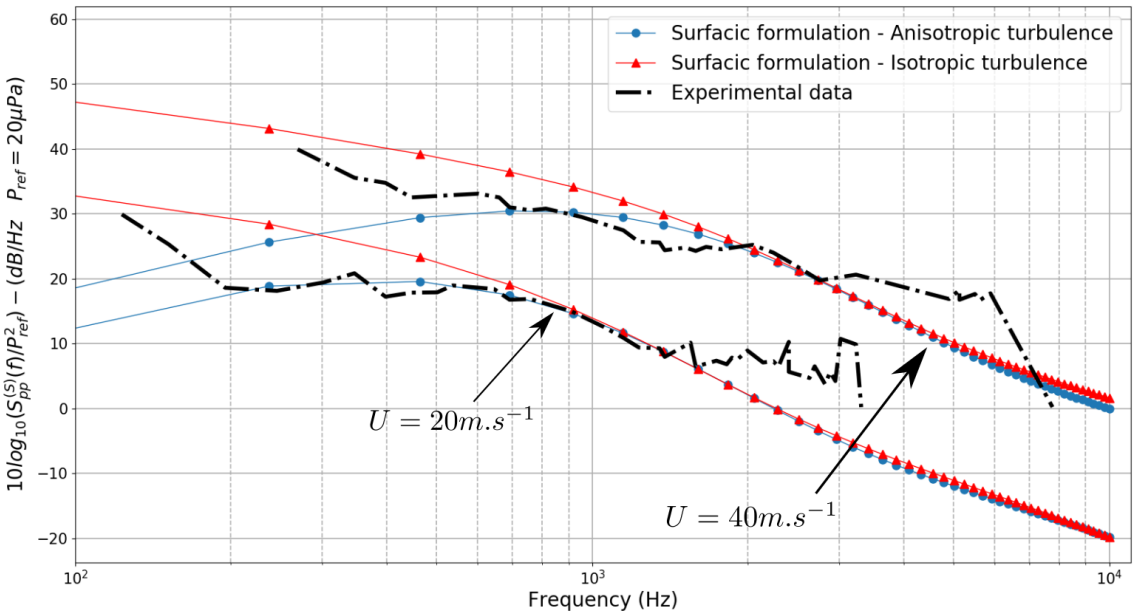

Figure 2: Sound pressure level (dB/Hz) for a receiver above the trailing edge at $r_x = 1.22\,m$ *at mid-span* ($\theta_x = \psi_x = \pi/2$) *and calculated using the surfacic formulation using two turbulence models for the half plane Green function and measured of Stalnov et al. [10].*

5. RESULTS

5.1. Impact of the isotropic assumption

The model derived by Chase [8] and described by Equation 13 has been implemented and applied to a NACA 0012 profile. The wall pressure spectrum is described by two models that we want to compare : the Blake-TNO model for an anisotropic turbulence, known to show good agreement with measurements [9, 10], and our simplified turbulence model which can be expressed in the physical space. The boundary layers parameters are obtained with a XFoil simulation in accordance with Lee [9] and Stalnov et al. [10]. The measurements were performed by Stalnov et al. for a NACA 0012 of chord $c = 0.2$ m and span $L = 0.45$ m, at zero angle of attack for various values of the mean velocity. The receivers are placed on an arc in the mid-span plane at a distance $R = 1.22m$ from the trailing edge. Figure 2 shows that the SPL obtained with the anisotropic turbulence model is in better agreement with the measurements at low frequencies, and that both models yield similar results at high frequencies.

5.2. Comparison between surfacic and volumic approaches

The volumic approach presented in this document, unlike the surfacic approach, makes more convenient the use of an arbitrary Green's function. For validation purposes, we chose here to consider the *half plane* and the *multiple scattering* Green functions respectively described by Equation 15 and Equation 16, into the two formulations. Figures 3 and 4 show the predicted and measured spectra for $U = 20m.s^{-1}$ and

$U = 40m.s^{-1}$. We observe that both formulations differ significantly, especially at high frequency. These differences can be attributed to the fact that $\widehat{\phi}_{22}^{(1)}$ used in the volumic formulation have been approximated using one-point statistics as explained in Section 4. Moreover, as shown by Howe [12], the multiple scattering correction causes an oscillation around the value of the half plane Green function.

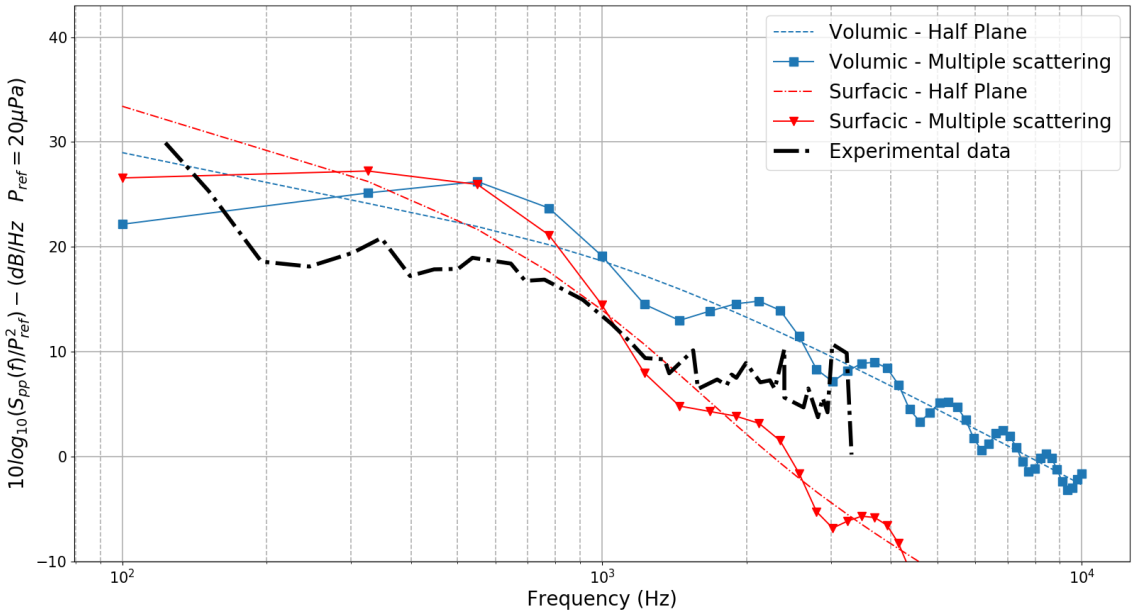

Figure 3: Sound pressure level (dB/Hz) for a receiver above the trailing edge at $r_x = 1.22$ m at mid-span ($\theta_x = \psi_x = \pi/2$) calculated using the volumic (Equation 12) and surfacic (Equation 13) approaches for the half plane and the multiple scattering Green functions, and measured by Stalnov et al. [10] for a mean velocity $U = 20m.s^{-1}$.

5.3. Directivity diagrams

Figure 5 shows the noise directivity for a receiver at mid-span and at $R = 1.22m$ from the edge. The frequency of 2700 Hz ($k_0c = 10$) has been chosen such that lobes appears using the multiple scattering Green function. It appears that the directivity of the Green function is retrieved, independently of the turbulence source. In fact, we observe that the same directivity is given by the jump of value in the Green function across the half-plane and the surfacic approach power spectral density on the one hand, and by the derivative of the Green function and the volumic approach power spectral density on the other hand. This is due to the fact that the half plane Green function cancels all contributions from sources that are not very close to the edge compared to the acoustic wavelength. Both approaches give the same number of lobes but show different behaviors in the direction opposite to the flow. The levels of the surfacic formulation are much lower than the levels of the volumic formulation at this frequency, as seen in Figure 3 and 4 for $\theta_x = \pi/2$.

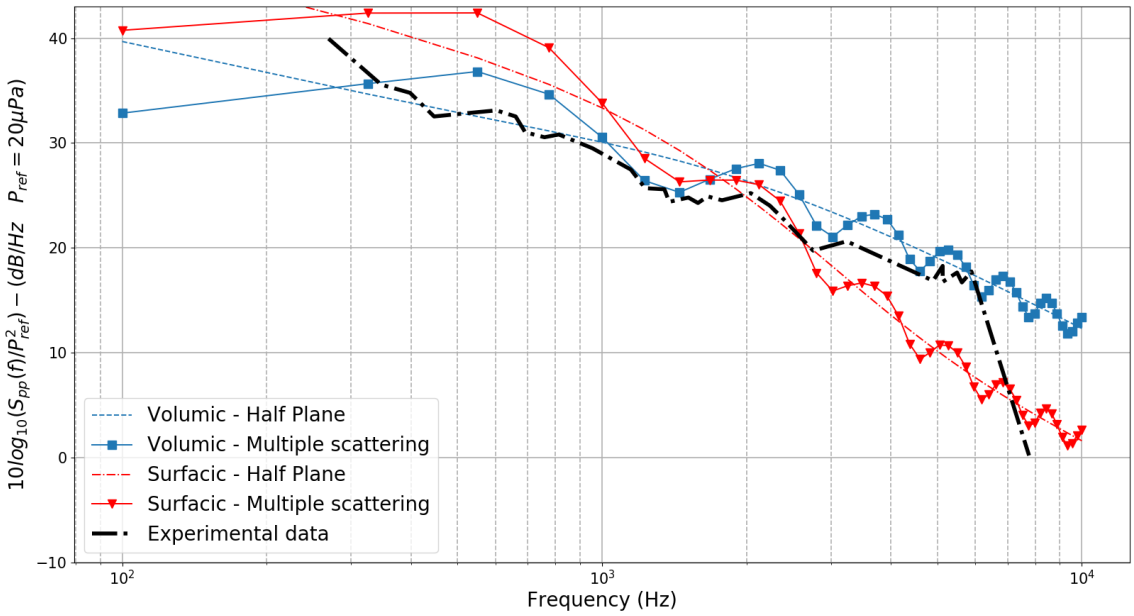

Figure 4: Sound pressure level (dB/Hz) for a receiver above the trailing edge at $r_x = 1.22$ m at mid-span ($\theta_x = \psi_x = \pi/2$) calculated using the volumic (Equation 12) and surfacic (Equation 13) approaches for the half plane and the multiple scattering Green functions, and measured by Stalnov et al. [10] for a mean velocity $U = 40m.s^{-1}$.

6. CONCLUSIONS

A semi-analytical prediction model of the broadband edge noise that can be used with the tailored Green function of an arbitrary geometry has been derived. As a first step, this volumic formulation has been compared to the surfacic formulation obtained from the diffraction theory for the same turbulence model in order to verify the obtained results. Some differences are observed at high frequencies in the spectra obtained with both formulation but the directivity diagrams are shown to be very similar.

Subsequently, by using the exact Green function tailored to the half plane, we will study the impact of the assumptions behind the half plane Green function and the diffraction theory. Considering trailing edge noise prediction, the anisotropy of the turbulent boundary layer has to be taken into account. Then, the volumic model will be extended to an arbitrary geometry using numerical simulations.

7. ACKNOWLEDGEMENTS

The authors would like to thank Naval Group and *Association Nationale Recherche et Technologie* (ANRT) for supporting this work.

8. REFERENCES

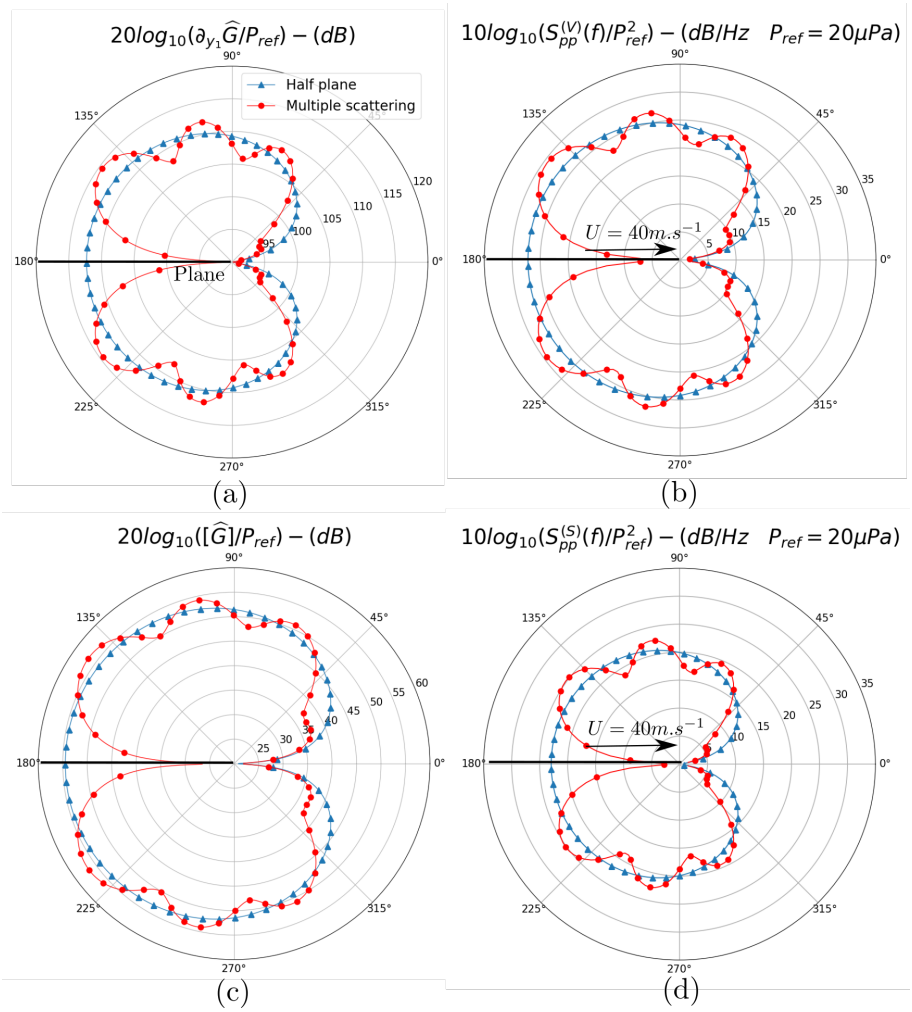

Figure 5: Directivity at $r_x = 1.22$ m at mid-span ($\psi_x = \pi/2$) and at $k_0 c = 10$ of (a) the derivative of the Green function in the flow direction, (b) the power spectral density of the acoustic pressure computed with the volumic formulation (Equation 12) at $U = 40m.s^{-1}$, (c) the jump of the value of the Green function across the half plane, (d) the power spectral density of the acoustic pressure computed with the surfacic formulation (Equation 13) at $U = 40m.s^{-1}$.

[1] K. L. Chandiramani. Diffraction of evanescent waves, with applications to aerodynamically scattered sound and radiation from unbaffled plates. *The Journal of the Acoustical Society of America*, 55, 1974.

[2] D. Chase. Noise radiated from an edge in turbulent flow. *AIAA Journal*, 13:1041–1047, 07 1975.

[3] M.S. Howe. Trailing edge noise at low mach numbers. *Journal of Sound and Vibration*, 225, 1999.

[4] P. E. Doak. Acoustic radiation from a turbulent fluid containing foreign bodies. *Proceedings of the Royal Society of London Series A Mathematical and Physical Sciences (1934-1990)*, 254, 04 1960.

[5] C.A. Albarracin, C. J. Doolan, R.F. Jones, C.H. Hansen, L.A. Brooks, and M.D. Teubner. A rans-based statistical noise model for trailing edge noise. *18th AIAA/CEAS Aeroacoustics Conference (33rd AIAA Aeroacoustics Conference)*, 06 2012.

[6] T. Takaishi, M. Miyazawa, and C. Kato. A computational method of evaluating non-compact sound based on the vortex sound theory. *The Journal of the Acoustical Society of America*, 121:1353–61, 04 2007.

[7] X. Gloerfelt; F. Pérot; C. Bailly; D. Juvé. Flow-induced cylinder noise formulated as a diffraction problem for low mach numbers. *Journal of Sound and Vibration*, 287, 2005.

[8] D. M. Chase. Sound radiated by turbulent flow off a rigid half-plane as obtained from a wavevector spectrum of hydrodynamic pressure. *The Journal of the Acoustical Society of America*, 52, 1972.

[9] S. Lee. Source characterization of turbulent boundary layer trailing edge noise using an improved tno model. *22nd AIAA/CEAS Aeroacoustics Conference*, 2016.

[10] O. Stalnov, C. Paruchuri, and P. Joseph. Towards a non-empirical trailing edge noise prediction model. *Journal of Sound and Vibration*, 372, 03 2016.

[11] N. Mathews, J.R.; Peake. An analytically-based method for predicting the noise generated by the interaction between turbulence and a serrated leading edge. *Journal of Sound and Vibration*, 422, 05 2018.

[12] M. S. Howe. Edge-source acoustic green's function for an airfoil of arbitrary chord, with application to trailing-edge noise. *The Quarterly Journal of Mechanics and Applied Mathematics*, 54, 02 2001.

[13] J E. Ffowcs Williams and L H. Hall . Aerodynamic sound generation by turbulent flow in the vicinity of a scattering half plane. *Journal of Fluid Mechanics*, 40:657 – 670, 03 1970.

[14] W.K. Blake. *Mechanics of Flow-Induced Sound and Vibration, Vol. I and II, in Applied Mathematics and Mechanics*. 2017.

[15] S. Glegg and W. Devenport. *Aeroacoustics of low mach number flows: Fundamentals, analysis, and measurement*. Academic Press, 02 2017.

[16] W.K. Blake. Turbulent velocity and pressure fields in boundary layer flows over rough surfaces. *Proceedings of the Symposium on Turbulence in Liquids*, 1971.

[17] G M. Corcos . The structure of the turbulent pressure field in boundary-layer flows. *Journal of Fluid Mechanics*, 18:353 – 378, 03 1964.

[18] H. Schlichting and K. Gersten. *Boundary layer theory*. Springer, 9th edition.